Published in IET Microwaves, Antennas & Propagation
Received on 12th February 2013
Revised on 31st October 2013
Accepted on 10th November 2013
doi: 10.1049/iet-map.2013.0086

ISSN 1751-8725

Bacterial foraging optimisation and method of moments for modelling and optimisation of microstrip antennas

Mounir Amir[1,2], Sami Bedra[1], Siham Benkouda[3], Tarek Fortaki[1]

[1]*Electronics Department, University of Batna, 05000 Batna, Algeria*
[2]*National Research Center of Welding and Non Destructive Testing, 16002 Algiers, Algeria*
[3]*Electronics Department, University of Constantine 1, 25000 Constantine, Algeria*
E-mail: mounir.amir@yahoo.fr

Abstract: A novel technique applying bacterial foraging optimisation (BFO) in conjunction with the method of moments (MOM) is developed to calculate accurately the resonant frequency and bandwidth of rectangular microstrip antenna of any dimension and of any substrate thickness. The resonant frequency results obtained by using (BFO/MOM) algorithm are in very good agreement with the experimental results available in the literature. The computation time is greatly reduced as compared with the classical MOM. Furthermore, the idea of this paper can be used for calculating the various parameters of microstrip antennas of different structures and geometries.

1 Introduction

Owing to their many attractive features and excellent advantages, microstrip antennas have attracted attention in both theoretical research and engineering applications over the past decades. Microstrip antennas are used in an increasing number of applications, ranging from biomedical diagnosis to wireless communication. Recent research on microstrip antennas is aimed at size reduction, high gain, resonant frequency, wide bandwidth, multiple functionality and system-level integration [1]. Several methods are available in the literature for computing the resonant frequency of patch antennas. These methods can generally be divided into two groups: simple analytical methods and rigorous numerical methods. The analytical methods, based on some fundamental simplifying physical assumptions regarding the radiation mechanism of antennas, are the most useful for practical design as well as providing a good intuitive explanation of the operation of microstrip antennas. However, these methods are not suitable and robust for many structures, in particular, if this antenna has a thick substrate. For rigorous methods such as the method of moments (MOM) the exact mathematical formulations involve extensive numerical procedures, thus requiring extensive computational time. Evolutionary algorithms, in particular the genetic algorithms (GA), have been widely used in electromagnetic applications in recent years [2, 3]. A new stochastic optimisation technique, particle swarm optimisation (PSO) has now gained popularity in the electromagnetic community. PSO can be understood as a modelling via an analogy similar to the social activities of a flock of birds, or a swarm of bees. PSO is a powerful technique that greatly simplifies the optimisation process compared with artificial neural networks and GA [4–6]. More recently, central force optimisation was introduced as a new deterministic metaheuristic for multi-dimensional search and optimisation based on the metaphor of gravitational kinematics; this algorithm was used for antenna optimisation in [7] and good results were obtained. Following the invention of bacterial foraging algorithm (BFOA) by Passino in 2002 [8], BFOA has gained increasing use. Bacterial foraging optimisation (BFO) is probabilistic based search and is free from derivatives [9].

In this paper, the combination of BFO and MOM is presented for the calculation of the resonant frequency and bandwidth of microstrip antennas. This combination leads to an important reduction of the computation time, and at the same time maintains the quality of the results obtained by the MOM. The same algorithm can be also beneficial for antenna designers for the optimisation of the geometrical parameters of a microstrip patch.

2 Analysis method

The problem to be solved is illustrated in Fig. 1. We have a rectangular microstrip patch of length 'a' along the 'x' direction and width 'b' along the 'y' direction over a ground plane. The metallic patch and the ground plane are assumed to be perfect electric conductors, with negligible thickness. The patch, is printed on an isotropic dielectric substrate of thickness 'd', which is characterised by the free space permeability 'μ_0' and a permittivity 'ε'. The ambient medium is air with constitutive parameters 'μ_0' and 'ε_0'.

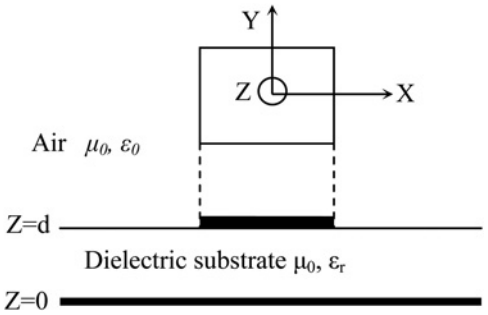

Fig. 1 *Geometrical structure of a rectangular microstrip patch*

Assuming an $e^{i\omega t}$ time variation and starting from Maxwell's equations in the Fourier transform domain, we can show that the transverse fields inside the jth layer ($Z_{j-1} < Z < Z_j$) can be written in terms of the longitudinal components $\tilde{E}_z$ and $\tilde{H}_z$ as [10, 11]

$$\tilde{\boldsymbol{E}}(k_s,\ z) = \begin{bmatrix} \tilde{E}_x(k_s,\ z) \\ \tilde{E}_y(k_s,\ z) \end{bmatrix} = \bar{\boldsymbol{F}}(k_s) \cdot \begin{bmatrix} \dfrac{1}{k_s}\dfrac{\partial \tilde{E}_z(k_s,\ z)}{\partial z} \\ \dfrac{\omega\mu_0}{k_s}\tilde{H}_z(k_s,\ z) \end{bmatrix} \tag{1}$$

$$\tilde{\boldsymbol{E}}(k_s,\ z) = \bar{\boldsymbol{F}}(k_s) \cdot \boldsymbol{e}(k_s,\ z)$$

$$\tilde{\boldsymbol{H}}(k_s,\ z) = \begin{bmatrix} \tilde{H}_y(k_s,\ z) \\ -\tilde{H}_x(k_s,\ z) \end{bmatrix} = \bar{\boldsymbol{F}}(k_s) \cdot \begin{bmatrix} \dfrac{\omega\varepsilon_j}{k_s}\tilde{H}_z(k_s,\ z) \\ \dfrac{1}{k_s}\dfrac{\partial \tilde{H}_z(k_s,\ z)}{\partial z} \end{bmatrix} \tag{2}$$

$$\tilde{\boldsymbol{H}}(k_s,\ z) = \bar{\boldsymbol{F}}(k_s) \cdot \boldsymbol{h}(k_s,\ z)$$

where $\boldsymbol{e}$ and $\boldsymbol{h}$ denote, respectively, the transverse electric and magnetic fields in the (TM, TE) representation, and

$$\bar{\boldsymbol{F}}(k_s) = \frac{1}{k_s}\begin{bmatrix} k_x & k_y \\ k_y & -k_x \end{bmatrix} \tag{3}$$

with $k_s^2 = k_x^2 + k_y^2$.

Substituting the expressions of $\tilde{E}_z$ and $\tilde{H}_z$ [10, 11] into (1) and (2), we obtain

$$\tilde{E}_z = \boldsymbol{A} \cdot e^{-ik_z Z} + \boldsymbol{B} \cdot e^{ik_z Z} \tag{4}$$

$$\tilde{H}_z = \bar{\boldsymbol{g}}(k_s) \cdot \left[\boldsymbol{A}.e^{-ik_z Z} - \boldsymbol{B} \cdot e^{ik_z Z}\right] \tag{5}$$

In (4) and (5), $\boldsymbol{A}$ and $\boldsymbol{B}$ are two-component unknown vectors and

$$\bar{\boldsymbol{g}}(k_s) = \mathrm{diag}\left[\frac{\omega\varepsilon}{k_z},\ \frac{k_z}{\omega\mu}\right] \tag{6}$$

Writing (4) and (5) in the planes $z = z_{j-1}$ and $z = z_j$ and by eliminating the unknowns $\boldsymbol{A}$ and $\boldsymbol{B}$, we obtain the matrix form

$$\begin{bmatrix} \boldsymbol{e}(k_s,\ z_j^-) \\ \boldsymbol{h}(k_s,\ z_j^-) \end{bmatrix} = \bar{\boldsymbol{T}}_j \cdot \begin{bmatrix} \boldsymbol{e}(k_s,\ z_{j-1}^+) \\ \boldsymbol{h}(k_s,\ z_{j-1}^+) \end{bmatrix} \tag{7}$$

with

$$\bar{\boldsymbol{T}}_j = \begin{bmatrix} \bar{\boldsymbol{T}}_j^{11} & \bar{\boldsymbol{T}}_j^{12} \\ \bar{\boldsymbol{T}}_j^{21} & \bar{\boldsymbol{T}}_j^{22} \end{bmatrix}$$
$$\bar{\boldsymbol{T}}_j = \begin{bmatrix} \cos(k_{zj}.d_j) & -i.\bar{\boldsymbol{g}}^{-1}.\sin(k_{zj}.d_j) \\ -i.\bar{\boldsymbol{g}}.\sin(k_{zj}.d_j) & \cos(k_{zj}.d_j) \end{bmatrix} \tag{8}$$

which combines $\boldsymbol{e}$ and $\boldsymbol{h}$ on both sides of the jth layer as input and output quantities. The matrix $\bar{\boldsymbol{T}}_j$ is the matrix representation of the jth layer in the (TM, TE) representation.

In the spectral domain, the boundary conditions for the structure shown in Fig. 1 are

$$\bar{\boldsymbol{e}}_1(k_s,\ z_0^+) = \bar{0} \tag{9}$$

$$\begin{bmatrix} \bar{\boldsymbol{e}}_2(k_s,\ z_1^+) \\ \bar{\boldsymbol{h}}_2(k_s,\ z_1^+) \end{bmatrix} = \bar{\boldsymbol{T}}_1 \cdot \begin{bmatrix} \bar{\boldsymbol{e}}_1(k_s,\ z_0^+) \\ \bar{\boldsymbol{h}}_1(k_s,\ z_0^+) \end{bmatrix} - \begin{bmatrix} 0 \\ \bar{\boldsymbol{J}}(z_1) \end{bmatrix} \tag{10}$$

$$\bar{\boldsymbol{h}}_2(k_s,\ z_1^+) = \bar{\boldsymbol{g}}_0(k_s).\bar{\boldsymbol{e}}_2(k_s,\ z_1^+) \tag{11}$$

The transformed components of the tangential electric field are expressed as a function of the transformed current density components on the patch, as

$$\begin{bmatrix} \tilde{E}_x \\ \tilde{E}_y \end{bmatrix} = \begin{bmatrix} G_{xx} & G_{xy} \\ G_{yx} & G_{yy} \end{bmatrix} \cdot \begin{bmatrix} \tilde{J}_x \\ \tilde{J}_y \end{bmatrix} \tag{12}$$

The Galerkin moment method is implemented in the Fourier transform domain to reduce the integral equation to a matrix equation. The surface current $\boldsymbol{J}$ on the patch is expanded into a finite series of known basis functions J_{xn} and J_{ym}

$$\boldsymbol{J} = \sum_{n=1}^{N} a_n \begin{bmatrix} J_{xn} \\ 0 \end{bmatrix} + \sum_{m=1}^{M} b_m \begin{bmatrix} 0 \\ J_{ym} \end{bmatrix} \tag{13}$$

where a_n and b_m are the mode expansion coefficients to be sought. Substituting the vector Fourier transforms of (13) into the integral equation. Next, the resulting equation is tested by the same set of basis functions that was used in the expansion of the patch current. Thus, the integral equation is decomposed into the following matrix equation

$$\begin{bmatrix} \left(\bar{Z}_{kn}^1\right)_{N\times N} & \left(\bar{Z}_{km}^2\right)_{N\times M} \\ \left(\bar{Z}_{lm}^3\right)_{M\times N} & \left(\bar{Z}_{\mathrm{ln}}^4\right)_{M\times M} \end{bmatrix} \cdot \begin{bmatrix} (a_n)_{N\times 1} \\ (b_n)_{M\times 1} \end{bmatrix} = \begin{bmatrix} \bar{0} \\ \bar{0} \end{bmatrix}$$

$$Z_{kn}^1 = \int_{-\infty}^{+\infty}\int_{-\infty}^{+\infty} \tilde{J}_{xk}(-k_x,\ -k_y) \cdot G_{xx}.\tilde{J}_{xm}(k_x,\ k_y)\mathrm{d}k_x\mathrm{d}k_y$$

$$Z_{km}^2 = \int_{-\infty}^{+\infty}\int_{-\infty}^{+\infty} \tilde{J}_{xk}(-k_x,\ -k_y) \cdot G_{xy}.\tilde{J}_{ym}(k_x,\ k_y)\mathrm{d}k_x\mathrm{d}k_y \tag{14}$$

$$Z_{lm}^3 = \int_{-\infty}^{+\infty}\int_{-\infty}^{+\infty} \tilde{J}_{yl}(-k_x,\ -k_y) \cdot G_{yx}.\tilde{J}_{xm}(k_x,\ k_y)\mathrm{d}k_x\mathrm{d}k_y$$

$$Z_{ln}^4 = \int_{-\infty}^{+\infty}\int_{-\infty}^{+\infty} \tilde{J}_{yl}(-k_x,\ -k_y) \cdot G_{yy}.\tilde{J}_{ym}(k_x,\ k_y)\mathrm{d}k_x\mathrm{d}k_y$$

doi: 10.1049/iet-map.2013.0086

The system of linear equations given in (14) has non-trivial solutions when

$$\det[\boldsymbol{Z}(\omega)] = 0 \tag{15}$$

Equation (15) is an eigenequation for ω, from which the characteristics of the planar structure of Fig. 1 can be obtained. In fact, let $\omega = 2\pi(fr + i\,fi)$ be the complex root of (15). In that case, the quantity fr stands for the resonant frequency, and the quantity $BW = 2fi/fr$ stands for the bandwidth. In our case (15) represents the function that will be optimised by using BFO algorithm.

3 Bacterial foraging optimisation

BFO is a new evolutionary computation technique which has been proposed by Passino [8, 12, 13]. It is inspired by the pattern exhibited by bacterial foraging behaviour. Bacteria have the tendency to gather to the nutrient-rich areas by an activity called chemotaxis. It is known that bacteria swim by rotating whip such as flagella driven by a reversible motor embedded in the cell wall. *Escherichia coli* has 8–10 flagella placed randomly on a cell body. When all flagella rotate counterclockwise, they form a compact, helix propelling the cell along a trajectory, which is called run. When the flagella rotate clockwise, they pull on the bacterium in different directions and cause the bacteria to tumble. The bacterial foraging system primarily consists of four sequential mechanisms, namely chemotaxis, swarming, reproduction and elimination-dispersal. A brief outline of each of these processes is given in this section.

3.1 Chemotaxis

An *E. coli* bacterium can move in two different ways: it can run (swim for a period of time) or it can tumble, and alternate between these two modes of operation in the entire lifetime. In the BFO, a unit walk with random direction represents a tumble and a unit walk in the same direction indicates a run. In computational chemotaxis, the movement of the ith bacterium after one step is represented as

$$\theta^i(j+1,\ k,\ l) = \theta^i(j,\ k,\ l) + C(i) + \phi(j) \tag{16}$$

where $\theta^i(j, k, l)$ denotes the location of ith bacterium at jth chemotactic, kth reproductive and lth elimination and dispersal step. $C(i)$ is the length of unit walk, which is a constant in basic BFO and $\phi(j)$ is the direction angle of the jth step. When its activity is run, $\phi(j)$ is the same as $\phi(j-1)$, otherwise, $\phi(j)$ is a random angle directed within a range of [0,2p]. If the cost at $hi(j+1, k, l)$ is better than the cost at $\theta^i(j, k, l)$ then the bacterium takes another step of size $C(i)$ in that direction otherwise it is allowed to tumble. This process is continued until the number of steps taken is greater than the number of chemotactic loop, N_c.

3.2 Swarming

The bacteria in times of stress release attractants to signal bacteria to swarm together. Each bacterium also releases a repellent to signal others to be at a minimum distance from it. Thus all of them will have a cell to cell attraction via attractant and cell to cell repulsion via repellent. The cell to cell signalling in *E. coli* swarm may be mathematically represented as

$$\begin{aligned} J_{cc}(\theta,\ P(j,\ i,\ l)) &= \sum_{i=1}^{N} J_{cc}(\theta,\ \theta^i(j,\ i,\ l)) \\ &= \sum_{i=1}^{N}\left[-d_a \exp\left(-w_a \sum_{m=1}^{P}\left(\theta_m - \theta_m^i\right)^2\right)\right] \\ &\quad + \sum_{i=1}^{N}\left[h_r \exp\left(-w_r \sum_{m=1}^{P}\left(\theta_m - \theta_m^i\right)^2\right)\right] \end{aligned} \tag{17}$$

where $J_{cc}(\theta, P(j, k, l))$ represents the objective function value to be added to the actual objective function, N is the total number of bacteria, p is the number of variables to be

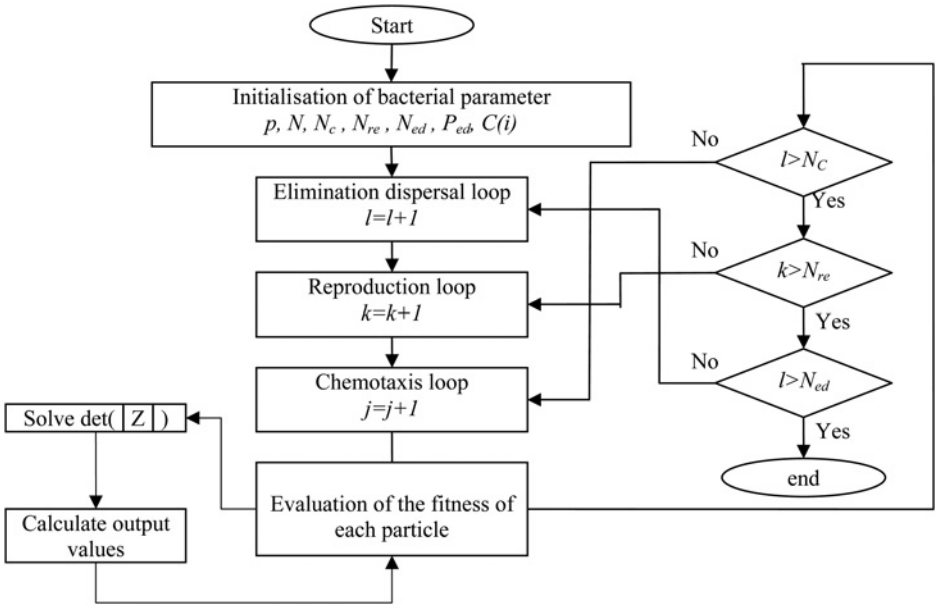

Fig. 2 *Flowchart of the BFO/MOM algorithm*

Table 1 Resonant frequency and bandwidth of rectangular microstrip antenna through multiple runs of the BFO/MOM code

Number of run	Resonant frequency, GHz	Bandwidth, %
1	4.496 932 496	1.091 076 910
2	4.496 900 295	1.089 652 592
10	4.496 925 697	1.090 776 181
11	4.496 904 242	1.089 827 161
20	4.496 935 154	1.091 194 475
21	4.496 937 398	1.091 293 727
30	4.496 900 985	1.089 683 087
31	4.496 900 244	1.089 650 334
40	4.496 904 371	1.089 832 870
41	4.496 904 339	1.089 831 458
50	4.496 905 884	1.089 899 778
51	4.496 903 676	1.089 802 130
60	4.496 911 738	1.090 158 753
61	4.496 912 159	1.090 177 375
70	4.496 911 331	1.090 140 723
71	4.496 914 646	1.090 287 359
80	4.496 908 786	1.090 028 136
81	4.496 905 622	1.089 888 207
90	4.496 912 167	1.090 177 714
91	4.496 919 235	1.090 490 352
98	4.496 900 283	1.089 652 044
99	4.496 900 613	1.089 666 660
100	4.496 915 523	1.090 326 131

optimised and $\theta = [\theta_1, \theta_2, \ldots, \theta_p]^T$ is a point in the p-dimensional search domain. d_a, w_a, h_r and w_r are coefficients to be chosen properly.

3.3 Reproduction

After all N_c chemotactic steps have been covered, a reproduction step takes place. The fitness values of the bacteria are sorted in ascending order. The lower half of the bacteria having higher fitness die and the remaining $Nr = N/2$ bacteria are allowed to split into two identical ones. Thus the population size after reproduction is maintained constant.

3.4 Elimination and dispersal

Since bacteria may stuck around the initial or local optimal positions, it is required to diversify the bacteria either gradually or suddenly so that the possibility of being trapped into local minima is eliminated. The dispersion operation takes place after a certain number of reproduction process. A bacterium is chosen, according to a pre-set probability $\boldsymbol{P}$, to be dispersed and moved to another position within the environment. These events may help to prevent the local minima trapping effectively, but unexpectedly disturb the optimisation process. The detailed of this concept is presented in [8].

The basic program flow of BFO/MOM is depicted in a flowchart as shown in Fig. 2. As mentioned, the objective of the optimisation in this work is the optimisation of the matrix impedance ($\boldsymbol{Z}$) in (15).

$P = 1$: dimension of the search space
$N = 50$: the number of bacteria in the population
$N_c = 50$: chemotactic steps
$N_{re} = 10$: the number of reproduction steps
$N_{ed} = 2$: the number of elimination-dispersal events
$P_{ed} = 0.25$: elimination-dispersal with probability
$C(i) = 0.05$: the size of the step taken in the random direction specified by the tumble.

4 Results

In [14], it is shown that application of BFO is suitable for any complicated antenna structure including an antenna array. Keeping this in mind, we hybridised BFO with the MOM for the calculation of the resonant frequency and bandwidth. For stochastic optimisations methods, the final solution can only be considered optimal by repetition of the results [15]. For a rectangular microstrip antenna with $a = 1.9$ cm, $b = 2.29$ cm, $d = 1.59$ mm and $\varepsilon_r = 3.32$, we have estimated the resonant frequency and bandwidth of this antenna by running the BFO/MOM code 100 times. In the interest of brevity, we show in Table 1 only some of them. It is clear from Table 1 that our BFO/MOM code gives almost the same results through multiple runs.

Table 2 Comparison of the calculated resonant frequency with measured and calculated data, for a rectangular microstrip antenna

a, cm	*b*, cm	*d*, cm	ε_r	Resonant frequencies, GHz	
				Measured	BFO /MOM
5.700	3.800	0.3175	2.33	2.310[a]	2.3208
1.080	3.400	1.281	2.55	3.150[a]	3.1927
1.265	3.500	1.281	2.55	2.980[a]	2.9871
0.920	3.130	1.200	2.55	3.470[a]	3.4902
1.170	1.280	0.300	2.50	6.570[a]	6.6209
1.530	1.630	0.300	2.50	5.270[a]	5.3164
0.910	1.000	0.127	10.2	4.600[a]	4.7119
5.700	3.800	0.3175	2.33	2.310[b]	2.3208
4.550	3.050	0.3175	2.33	2.890[b]	2.8225
2.950	1.950	0.3175	2.33	4.240[b]	4.1179
1.950	1.300	0.3175	2.33	5.840[b]	5.7534
1.700	1.100	0.1375	2.33	6.800[b]	6.6877
1.400	0.900	0.3175	2.33	7.700[b]	7.6360
1.200	0.800	0.3175	2.33	8.270[b]	8.1060
1.050	0.700	0.3175	2.33	9.140[b]	9.1870
1.700	1.100	0.9525	2.33	4.730[b]	4.5026
1.700	1.100	0.1524	2.33	7.870[b]	7.7110
4.100	4.140	0.1524	2.50	2.228[c]	2.2014
6.858	4.140	0.1524	2.50	2.200[c]	2.1148
10.80	4.140	0.1524	2.50	2.181[c]	2.1173
2.000	2.500	0.0790	2.22	3.970[d]	3.7141
1.120	1.200	0.2420	2.55	7.050[d]	7.0224
0.790	1.255	0.4000	2.55	7.134[d]	7.1287

[a]These frequencies calculated by Gollapudi *et al.* [9] using VMBFO Technique.
[b]These frequencies measured by Chang *et al.* [16].
[c]These frequencies measured by Carver [17].
[d]Measured by Kara [18, 19].

Table 3 Comparison of the calculated bandwidth with measured and calculated data, for a rectangular microstrip antenna

a (cm)	*b* (cm)	*d* (mm)	ε_r	Bandwidth, %		
				Measured	Curve fitting	BFO/ MOM
5.7	3.8	3.175	2.33	3.117[a]	4.988	4.601
4.55	3.05	3.175	2.33	4.083[a]	6.143	5.758
1.05	0.7	3.175	2.33	23.850[a]	—	26.557
1.7	1.1	1.524	2.33	6.607[a]	8.212	7.863
1.9	2.29	1.59	2.32	2.17[b]	—	2.714

[a]These bandwidths measured by Chang *et al.* [16].
[b]This bandwidth measured by Bahl *et al.* [20].

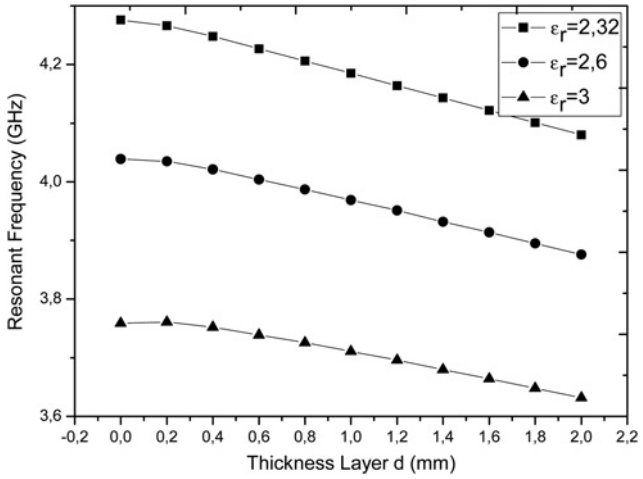

Fig. 3 *Resonant frequency against electrical substrate thickness using BFO/MOM algorithm*

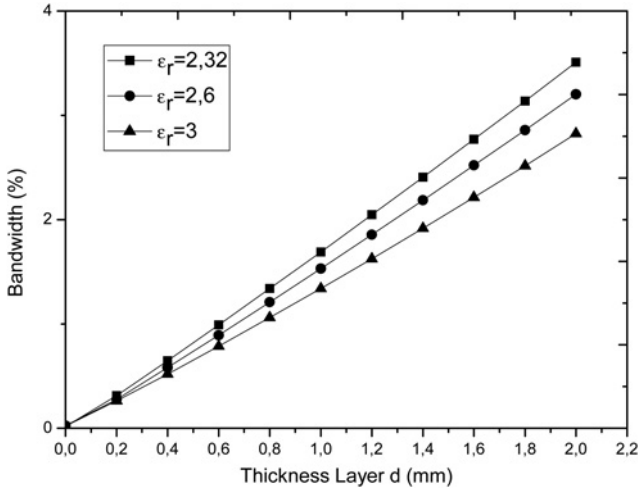

Fig. 4 *Bandwidth against electrical substrate thickness using BFO/MOM algorithm*

The resonant frequencies and bandwidths calculated by using the BFO/MOM algorithm presented in this paper for electrically thin and thick rectangular MSAs are listed and compared with measured results in Tables 2 and 3, respectively. In Table 3, we have also presented calculated bandwidths obtained via the curve fitting formulae of Chew [21, 22]. The results of this method are in very good agreement with measurements. It can be very useful for the development of fast CAD algorithms.

Figs. 3 and 4 show the resonant frequency and bandwidth as a function of substrate thickness for different values of dielectric constant $\varepsilon_r = 2.32$, 2.6 and 3 of a rectangular patch antenna with dimensions $a = 1.9$ cm, $b = 2.29$ cm. From these graphs we see that the results obtained by BFO/MOM algorithms have the same behaviour as those obtained by the MOM. It is evident from Fig. 3 that the resonant frequency decreases as the antennas become electrically thicker as has been shown in previously published results [16].

To show the time-efficiency of the proposed methodology, we compare in Table 4 the time necessary for estimating the resonant frequency and bandwidth of the antenna by BFO/MOM with the one of the traditional MOM. The comparison is done for five different structures. The comparison in Table 4 shows that the CPU time required by the traditional moment method is higher approximately six times than that of the BFO/MOM.

Although we have presented in Section 4 only results for the TM_{01} mode, the BFO/MOM code developed in this paper can also give results for higher order modes. If we compare our BFO/MOM code with the electromagnetic simulator 'Ensemble', which is also based on the full-wave moment method, we can say that our code has the best speed (the setup time required to input the problem geometry and parameters for 'ensemble' takes few minutes). Another disadvantage of 'ensemble' is that it is much slower in computing the resonant frequencies of higher order modes than the resonant frequency of the fundamental mode [23]. This not the case of the BFO/MOM code since the number of basic functions used in the approximation of the current in the fundamental mode is similar to that used in higher order modes.

5 Conclusions

An efficient method for the integration of BFO with the MOM for microstrip antenna modelling has been presented. BFO/MOM was applied successfully for the determination of resonant frequency and bandwidth of a rectangular patch antenna. The calculated results have been compared with measured ones available in the literature and excellent agreement has been found. In addition, the improvement in the processing time compared with the conventional moment method is demonstrated. The proposed algorithm seems to be robust and effective soft computing tool for engineering design antennas problems.

6 References

1 Neag, D.K., Pattnaik, S., Panda, D.C., Devi, S., Khuntia, B., Dutta, M.: 'Design of a wideband microstripe antenna and the use of artificial neural networks in parameter calculation', *IEEE Trans. Antennas Propag.*, 2005, **45**, (3), pp. 60–65

Table 4 Comparison between results and CPU time of traditional moment method with BFO/MOM

a, cm	*b*, cm	*d*, mm	ε_r	Traditional moment method			BFO/MOM		
				Fr, GHz	BW, %	CPU time, s	*Fr*, GHz	BW, %	CPU time, s
1.5	1	1	10.3	4.4971	1.1014	297.98	4.4969	1.0900	48.05
1.5	1	1	11.6	4.2461	0.9407	300.86	4.2459	0.9393	47.14
3.4	3	3.175	2.62	3.2429	0.2254	372.59	3.2426	0.1894	51.85
1.9	2.29	1.59	2.32	4.1162	2.7144	335.96	4.1160	2.6720	49.59
1.265	3.5	12.81	2.55	2.3499	15.0577	266.13	2.3500	15.0632	50.26

2 Selleri, S., Mussetta, M., Pirinoli, P., Zich, R.E., Matekovits, L.: 'Some Insight over new variations of the particle swarm optimization method', *IEEE Antennas Wirel. Propag. Lett*., 2006, **5**, (1), pp. 235–238

3 Josan, S.K., Sohal, J.S., Dhaliwal, B.S.: 'Design of elliptical microstrip patch antenna using genetic algorithms'. Proc. IEEE Int. Conf. Communication Systems, November 2012, pp. 140–143

4 Chung, K.L., Tam, W.Y.: 'Particle swarm optimization of wideband patch antennas'. Proc. Asia-Pacific Microwave Conf., December 2008, pp. 16–20

5 Deb, A., Gupta, B., Roy, J.S.: 'Performance comparison of differential evolution, genetic algorithm and particle swarm optimization in impedance matching of aperture coupled microstrip antennas'. 11th Mediterranean Microwave Symp., September 2011, pp. 17–20

6 Guney, K., Sarikaya, N.: 'Comparison of adaptive-network-based fuzzy inference systems for bandwidth calculation of rectangular microstrip antennas', *Expert Syst. Appl.*, 2009, **36**, (2), pp. 3522–3535

7 Mahmoud, K.R.: 'Central force optimization: Nelder-Mead hybrid algorithm for rectangular microstrip antenna design', *Electromagnetics*, 2011, **31**, (8), pp. 578–592

8 Passino, K.M.: 'Biomimicry of bacterial foraging for distributed optimization and control', *IEEE Control Syst. Mag.*, 2002, **22**, (3), pp. 52–67

9 Gollapudi, S.V.R.S., Pattnaik, S.S., Bajpai, O.P., Devi, S., Bakwad, K.M.: 'Velocity Modulated Bacterial Foraging Optimization technique (VMBFO)', *Appl. Soft Comput.*, 2011, **11**, (1), pp. 154–165

10 Pozar, D.M.: 'Radiation and scattering from a microstrip patch on a uniaxial substrate', *IEEE Trans. Antennas Propag*., 1987, **35**, (6), pp. 613–621

11 Fortaki, T., Khedrouche, D., Bouttout, F., Benghalia, A.: 'A numerically efficient full-wave analysis of a tunable rectangular microstrip patch', *Int. J. Electron.*, 2004, **91**, (1), pp. 57–70

12 Mishra, S.: 'A hybrid least square-fuzzy bacteria foraging strategy for harmonic estimation', *IEEE Trans. Evol. Comput*., 2005, **9**, (1), pp. 61–73

13 Mishra, S., Panigrahi, B.K., Tripathy, M.: 'A hybrid adaptive-bacterial-foraging and feedback linearization scheme based D-STATCOM'. Proc. Int. Conf. Power System Technology, Singapore, November 2004, pp. 275–280

14 Mangaraj, B.B., Misra, I.S., Barisal, A.K.: 'Optimizing included angle of symmetrical V-dipoles for higher directivity using bacteria foraging optimization algorithm', *Prog. Electromagn. Res. B*, 2008, **3**, pp. 295–314

15 Goldberg, D.E.: 'Genetic algorithms in search, optimization and machine learning' (Addison-Wesley Longman Publishing Co., 1989)

16 Chang, E., Long, S.A., Richards, W.F.: 'An experimental investigation of electrically thick rectangular microstrip antennas', *IEEE Trans. Antennas Propag*., 1986, **34**, (6), pp. 767–772

17 Carver, K.R.: 'Practical analytical techniques for the microstrip antenna'. Proc. Workshop on printed Circuit antenna technology, New Mexico State University, Las Cruces, USA, October 1979, pp. 7.1–7.20

18 Kara, M.: 'The resonant frequency of rectangular microstrip antenna elements with various substrate thicknesses', *Microw. Opt. Technol. Lett*., 1996, **11**, (2), pp. 55–59

19 Kara, M.: 'Closed-form expressions for the resonant frequency of rectangular microstrip antenna elements with thick substrates', *Microw. Opt. Technol. Lett.*, 1996, **12**, (3), pp. 131–136

20 Bahl, I.J., Bhartia, P., Stuchly, S.S.: 'Design of microstrip antennas covered with a dielectric layer', *IEEE Trans. Antennas Propag*., 1982, **30**, (2), pp. 314–318

21 Chew, W.C., Liu, Q.: 'Resonance frequency of a rectangular microstrip patch', *IEEE Trans. Antennas Propag*., 1988, **36**, (8), pp. 1045–1056

22 Chew, W.C., Liu, Q.: 'Correction to 'Resonance frequency of a rectangular microstrip patch', *IEEE Trans. Antennas Propag.*, 1988, **36**, (12), pp. 1827

23 Losada, V., Boix, R.R., Horno, M.: 'Resonant modes of circular microstrip patches in multilayered substrates', *IEEE Trans. Microw. Theory Tech*., 1999, **47**, (4), pp. 488–498

doi: 10.1049/iet-map.2013.0086